European Polymer Journal 83 (2016) 77–88

Contents lists available at ScienceDirect

European Polymer Journal

journal homepage: www.elsevier.com/locate/europolj

Macromolecular Nanotechnology

Plasticizers assisted, shear-induced domino-assembly of nanofibrous polyaniline in PP matrix

Ming-Jer Tsai [a], Po-Hao Tseng [b], Yen-Zen Wang [c], Tar-Hwa Hsieh [a], Yu-Pei Chen [d], Yu-Shiang Shen [a], Ko-Shan Ho [a,*], Che-Kuei Chang [a]

[a] Department of Chemical and Materials Engineering, National Kaohsiung University of Applied Sciences, 415, Chien-Kuo Road, Kaohsiung 807, Taiwan
[b] Graduate Institute of Electrical Engineering, National Taiwan University, No. 1, Sec. 4, Roosevelt Road, Taipei 10617, Taiwan
[c] Department of Chemical and Materials Engineering, National Yun-Lin University of Science and Technology, 640 Yun-Lin, Taiwan
[d] TaiFlex Scientific Co., LTD, Taiwan

ARTICLE INFO

Article history:
Received 19 May 2016
Received in revised form 31 July 2016
Accepted 14 August 2016
Available online 16 August 2016

Keywords:
Polyaniline
Polyblend
Shearing
Domino

ABSTRACT

A nanofibrous polyaniline (PANFDBZnSt) was easily prepared when aniline monomers are polymerized in the presence of both n-dodecylbenzenesulfonic acid (DBSA) and zinc stearate ($Zn(St)_2$). The obtained PANFDBZnSt can be melt-mixed with PP matrix plasticized by both DBSA and $Zn(St)_2$ (PPDBZnSt) at 150 °C with shear rate as low as 40 rpm. During melt-mixing, the hairy-rod PANFDBZnSt blended with some of PPDBZnSt are able to self-assemble into rectangular layers that line up into erected domino-like structure in the PPDBZnSt matrix at higher shear rates. The intermolecular conjugation length of PANFDBZnSt molecules inside of the dominos is increased due to the shear-induced self-assembly and additional λ_{max} was found in the Near-IR range when shear rates were higher than 40 rpm. SEM and AFM micrographs show that pieces of dominos grow from the polyblend with shear rate higher than 40 rpm but some of the plasticizers (DBSA & $Zn(St)_2$) and PANFDBZnSt are spun out of the domino-structure at shear rate higher than 100 rpm. DSC thermograms demonstrate additional melting point contributed from the domino morphology. The IR-spectra reveal the formation of dominos come from the alkyl affinity between DBSA, $Zn(St)_2$ that belonged to both PANFDBZnSt and PPDBZnSt. X-ray diffraction patterns indicate the (1 1 1) plane of PP in the polybelnds was depressed at high shear rates. The rectangular layers of PANFDBZnSt inside of dominos contribute to new diffraction peak at lower angle which shifts to higher angle when some PANFDBZnSt molecules slip out with the lubrication of DBSA or $Zn(St)_2$ plasticizers at shear rates higher than 100 rpm.

1. Introduction

The blending of protonic-aid doped polyaniline with other matrix polymers or nanoclays has been studied for several years [1–7]. However, the conductivity, processing, and other properties of the resultant conducting polyblends were not improved due to the intractable nature of doped polyaniline molecules in the matrix polymers, resulting from its strong intra– or inter molecular positive and negative interaction and potential H-bondings. Ho et al. [8–10] prepared $Zn(DBSA)_2$

* Corresponding author.
E-mail address: hks@cc.kuas.edu.tw (K.-S. Ho).

http://dx.doi.org/10.1016/j.eurpolymj.2016.08.016
0014-3057/

from neutralization of ZnO with excess DBSA to avoid the solidification of the zinc salts product which was able to plasticize ES type polyaniline and improve the compatibility with PP by melt-mixing. The zinc salts were found to be good secondary dopants (protonic acid which can firmly dope with EB by acid-base neutralization is called primary dopant) for polyaniline but the obtained polyblends became too sticky to apply due to the presence of lots of undoped, free DBSAs which were used to prepare $Zn(DBSA)_2$ via the neutralization reaction with ZnO.

Aniline monomers can be emulsion-polymerized into nanofibers in the presence of DBSA which behaves as both part of the dopant and emulsifying agents [11–16]. In this study, we will try to introduce the long alkylated dispersing agent ($Zn(St)_2$) into polyaniline during the polymerization to depress its processing temperature, which made its melt-blending with PP possible in a plastograph mixer. The matrix PP will be plasticized with DBSA and $Zn(St)_2$ as well to decrease its melt-processing temperature to as low as 150 °C to avoid the possible thermal degradation of PANFs during melt-mixing.

The procedures of blending was set to melt-mix PANFDBZnSt with PP which was first plasticized by both DBSA and $Zn(St)_2$ at 170 °C to effectively depress the processing temperature to 150 °C at which the PANF was introduced. Surprisingly, lots of erected domino-like slabs were found to grow ubiquitously and rooted on the polyblend matrix when the shear rate was over 40 rpm at 150 °C. We understand this peculiar morphology has some connections with the nanofibrous structure since it was never found in the blending of regular polyaniline with PP [10] or other polymers [17,18]. In this paper, we will present how the dominos depend on the shear rate and how morphologies, and degree of conjugation of the polyblends vary with shear rate by UV-Vis-NIR, IR spectra, SEM, AFM, DSC thermograms, and X-ray diffraction patterns, respectively.

2. Experimentals

2.1. Preparation of PANFDBZnSt

Similar to regular polymerization method, 12 mL (0.127 mol) aniline (TOKYO KASEI KOGYO CO.), 21 g (0.0637 mol) DBSA (TOKYO KASEI KOGYO CO.) and 28 g (0.044 mol) $Zn(St)_2$ which can be uniformly distributed in water with the help of water soluble DBSA. And 160 mL distilled water were mixed and mechanically stirred in a 250 mL four-necked flask in an ice-bath with purging nitrogen drop wise with an ammonium peroxodisulfate (APS: SHOWA CHEMICALS INSTRUMENT CO.) aqueous solution (17 g or 0.075 mol of APS in 30 mL distilled water). To avoid a rise of the reaction temperature during polymerization, the polymerization was initiated APS aqueous solution at 0–5 °C, which persisted for 1 h. The obtained polyaniline was then poured into in a 750 mL acetone bath, followed by filtration and dried in vacuum at 40 °C for 24 h. The obtain nanofibrous polyaniline is named as PANFDBZnSt (polyaniline nanofibers of DBSA/$Zn(St)_2$) and the yield was estimated to be around 80%.

A comparison polymerization of aniline was performed on the same conditions in the absence of zinc stearate ($Zn(St)_2$). The obtained polyaniline nanofiber is named as PANFDB.

Aniline monomers were purified by vacuum distillation in a rotary evaporator and stored in a refrigerator before polymerization. DBSA, APS, and $Zn(St)_2$ were used directly without further purification.

2.2. Preparation of polylends and torque measurement in a plastograph mixer

30 g of PP is sheared and melted in a PLASTOGRAPH® mixer (Brabendar with W50 EHT type of mixer) at 170 °C until the torque reached the equilibrium value. And another 1.5 g (0.0461 mol) of DBSA and 2.25 g (0.0353 mol) $Zn(St)_2$ were added and shear-mixed for 15 min at 120 rpm, then cooled to 150 °C. 10g of PANFDBZnSt was added and shear-mixed for 20 min at selected shear rates ranged from 40 to 140 rpm. The prepared polyblend is called PANFDBZnSt/PPDBZnSt. The shear-experiments in the Brabendar in the presence of only plasticizer of DBSA or $Zn(St)_2$ was carried out as well for comparison. The torque (in N/m) developed during melt-mixing for all samples were recorded vs time in min.

PP was melt-mixed with either DBSA or $Zn(St)_2$ for comparison in the Brabendar and named as PPDB and PPZnSt, respectively.

PP was obtained from LCY Chemical Corp. with MI value of 27 and Tm of 172 °C, respectively.

2.3. UV-Vis-NIR spectroscopy

PANFDBZnSt and various PANFDBZnSt/PPDBZnSt polyblends were crushed and ground into powders in a mortar after treated with liquid N_2. The obtained powders were mixed with grease and ground into a uniform paste in a mortar, part of which was coated on a quartz plate for UV measurement. The UV-Vis-NIR spectra of PANFDBZnSt and various PANFDBZnSt/PPDBZnSt were obtained from a Hitachi U-2001 and DTS-1700 NIR Spectrometer. The scanning wavelength ranged from 300 to 1000 nm.

2.4. SEM (Scanning Electronic Microscopy)

PANFDB, PANFDBZnSt, PPDB, PPZnSt, and PANFDBZnSt/PPDBZnSt obtained from melt-mixing were prepared from strewn on carbonic tape and followed by posting on ferric stage. All samples were surface-plated with gold in a CVD process to

improve the surface conductivity for obtaining higher resolution. Their images were taken in a Field Emission SEM, HRSEM (HITACHI S-4200) with an accelerating voltage of 15 kV).

2.5. AFM (atomic forced microscopy)

PANFDBZnSt/PPDBZnSt prepared at 40, 100, and 140 rpm, respectively were melt-cast on a steel plate, cooled to room temperature, and separated for surface morphological studies by Atomic Forced Microscopic measurement (AFM (CSPM 4000)) operated in tapped mode. The software applied to analyze the image is Imager 4.7

2.6. FTIR spectroscopy

The functional groups of PANFDBZnSt and PANFDBZnSt/PPDBZnSt were characterized by FTIR spectroscopy with ATR attachment. The FTIR spectra were recorded on an IFS3000 v/s Fourier-transform infrared spectrometer at room temperature scanned from 4000 to 400 cm^{-1} with a resolution of 4 cm^{-1} and 16 numbers of scanning.

2.7. Differential scanning calorimetry (DSC)

DSC thermograms were obtained by Perkin-Elmer DSC-7 scanned from 50 °C to 200 °C at 10 °C/min in purging N_2. The weight was about 10 mg each and the temperature and heat of fusion of the DSC were calibrated by indium standard before using.

2.8. Powder method X-ray diffraction

The crystalline patterns of PPDBZnSt and PANFDBZnSt/PPDBZnSt powders were obtained from X-ray diffraction. An copper target (Cu Kα) Rigaku X-ray source with a wavelength of 1.5402 Å was used for diffraction. The scanning angle (2θ) started from 5° to 30° with a voltage of 40 kV and a current of 30 mA at 1 min^{-1}.

2.9. Resistivity measurement

The liquid N_2 frozen PANFDBZnSt/PPDBZnSt samples were first ground in a mortar into pellets which were compressed into a tablet whose thickness (t) and area (A) were measured at room temperature. A 4-probes Milliohm meter was used to measure their resistance (R) and resistivity (ρ) in Ω cm was calculated from the following equation:

$$\rho = RA/t$$

3. Results and discussion

3.1. Shear effect

The shearing effects on the blending of PANFDBZnSt and PP which was prepared in the presence of DBSA or $Zn(St)_2$ plasticizers were monitored by applying torque vs. shear time as demonstrated in Fig. 1 which illustrates stable equilibrium tor-

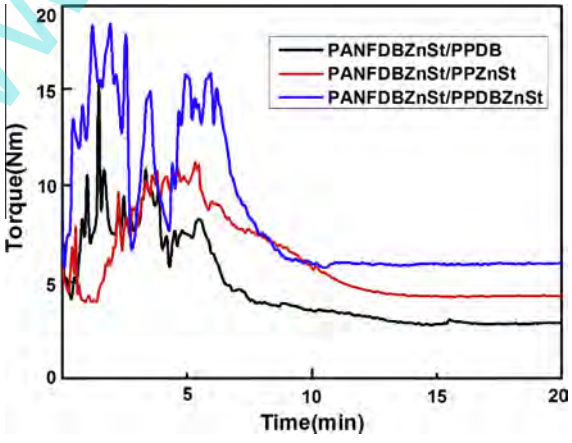

Fig. 1. Shear torque vs shear time of PANFDBZnSt/PP with different plasticizers.

ques are obtained after 10 min mixing for each sample and no significant thermal degradation was found (no significant torque fluctuation was found) until 20 min as low as 150 °C. PPs which are plasticized with pure DBSA, $Zn(St)_2$, and mixture of both DBSA and $Zn(St)_2$, respectively were mixed with PANFDBZnSt in the melt-mixer. And these polyblend systems are named as PANFDBZnSt/PPDB, PANFDBZnSt/PPDB, and PANFDBZnSt/PPDBZnSt, respectively. The stable equilibrium torques found for all polyblend systems after 10 min mixing indicated that PANFDBZnSt is compatible with various PP matrix plasticized with either DBSA or $Zn(St)_2$ through the alkyl affinity of the DBSA or $Zn(St)_2$ which are already present in PANFDBZnSt as depicted in Scheme 1. On the contrary, when both DBSA and $Zn(St)_2$ are present during melt-mixing, the obtained PANFDBZnSt/PPDBZnSt polyblend demonstrated the highest equilibrium torque. The highest equilibrium torque of PANFDBZnSt/PPDBZnSt than that of either PANFDBZnSt/PPDB or PANFDBZnSt/PPZnSt in Fig. 1 reveals the highest obstruction was present during melt-mixing, which is related to both DBSA and $Zn(St)_2$. In other words, the DBSA and $Zn(St)_2$ jointly lubricate PP matrix and help PANFDBZnSt molecules to mix with PP matrix and created new barrier force during melt-mixing. The increased torque force must involve the rearrangements of PANFDBZnSt which owns a nanofibrous structure and is easy to shear-assemble in the polymer matrix under high shear force with the lubrication effect provided by DBSA and $Zn(St)_2$ during melting mixing at high shear rates. However, the shear-induced assembly in the PANFDBZnSt/PPDBZnSt system was different from conventional aggregation, it assembled into rectangular layers which became ordered and were packed with each other into erected dominos rooted in PPDBZnSt matrix (will be shown in SEM and AFM micrographs) as demonstrated in Scheme 2. With the assistance of both shear power and plasticizer lubrication, these PANFDBZnSt molecules are able to stand up and pack into almost perpendicular dominos, which will interfere with each other during shearing and created additional barrier force, significantly increasing the equilibrium torque as illustrated in Fig. 1.

3.2. Degree of conjugation of PANFDBZnSt in PPDBZnSt matrix

The high degree of conjugation of PANFDBZnSt can be significantly monitored by the appearance of λ_{max} in the NIR region of PANFDBZnSt/PPDBZnSt at high shear rate as demonstrated in Fig. 2. We can clearly see the growing λ_{max} in the NIR region with shear rate, indicating highly self-assembling for PANFDBZnSt molecules inside erected dominos as depicted in Scheme 2. The alignment of these PANFDBZnSt inside of the erected dominos enhanced the intermolecular conjugation of PANFDBZnSt molecules when the shear rate is higher than 80 rpm according to Fig. 2 where clear λ_{max} in the NIR region can be seen. The driving force behind the alignment of these nanofibers originated from the alkyl affinity of DBSA and Zn $(St)_2$ both of which are present in both PANFDBZnSt and PPDBZnSt' which will be characterized by IR-spectra. They served as coupling agents for the assembly of PANFDBZnSt in the PPDBZnSt matrix into dominos d shearing force. However, too high shear rate can also cause the loss of some of PANFDBZnSt and most of plasticizers inside of dominos from the matrix [12] as described in Scheme 3. The spinning out effect deterred the building of thick dominos and stopped the λ_{max} red-shifting in the NIR regions when shear rate is higher than 100 rpm as seen in Fig. 2.

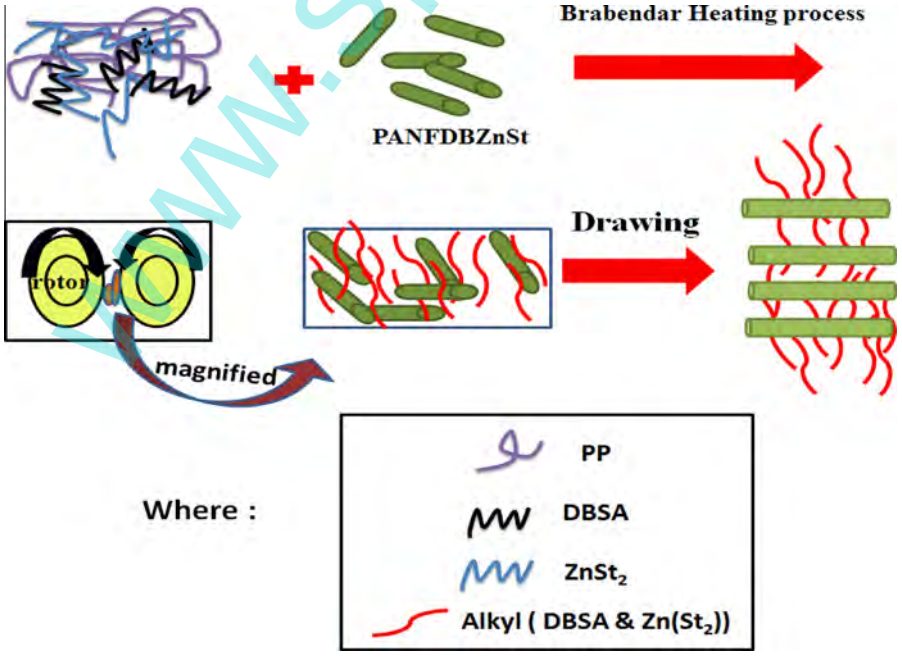

Scheme 1. Plasticizing process of DBSA, $Zn(St)_2$, and PP on PANFDBZnSt.

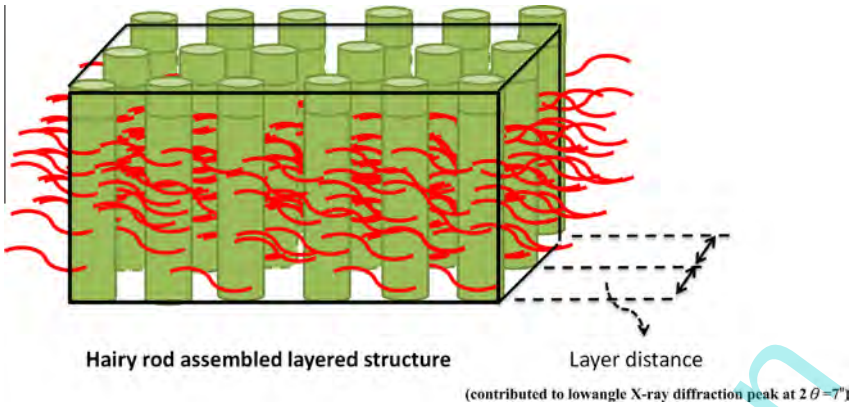

Scheme 2. Shear formed domino of hairy rod layered structure of PANFDBZnSt.

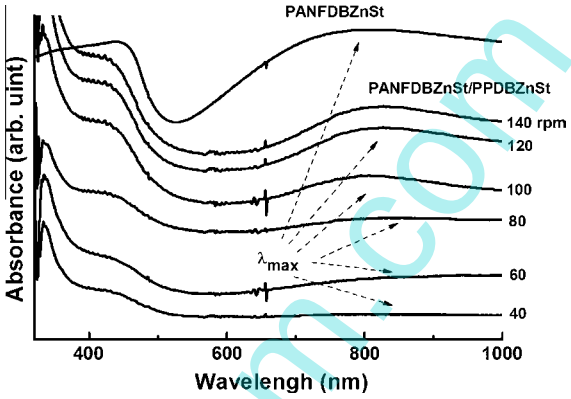

Fig. 2. UV-Vis-NIR spectra of PANFDBZnSt and PANFDBZnSt/PPDBZnSt at various shear rates.

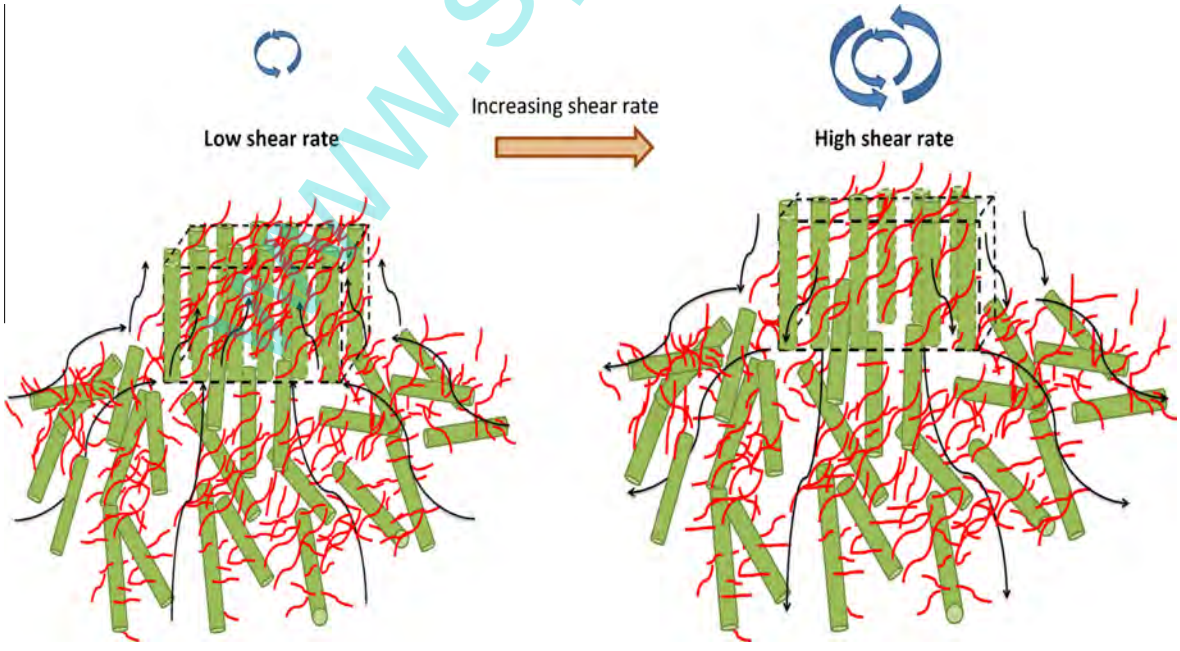

Scheme 3. Shear induced assembly and spinning off of PANFDBZnSt and alkyl plasticizers.

3.3. Electronic microscopic picture

3.3.1. SEM

The SEM and in-set TEM micrographs of PANFDB and PANFDBZnSt revealed the nanofibrous morphology in Fig. 3(a) and (b), which illustrates PANF molecules are prone to assembling due to the high aspect ratio of nanofibrous configuration. No significant ordered morphology can be found for those SEM pictures for neat PP, PPDB, and PPZnSt before blending with PANFDBZnSt as demonstrated in Fig. 3(c)–(e), respectively. Once PANF is added in the mixture of PPZnSt, lots of fragile porous flakes were formed and distributed randomly illustrated in Fig. 3(f). It is an evidence that PANFDBZnSt was able to combine with the PP molecules to create some ordered structure with the help of $Zn(St)_2$, which also means PANFDBZnSt is

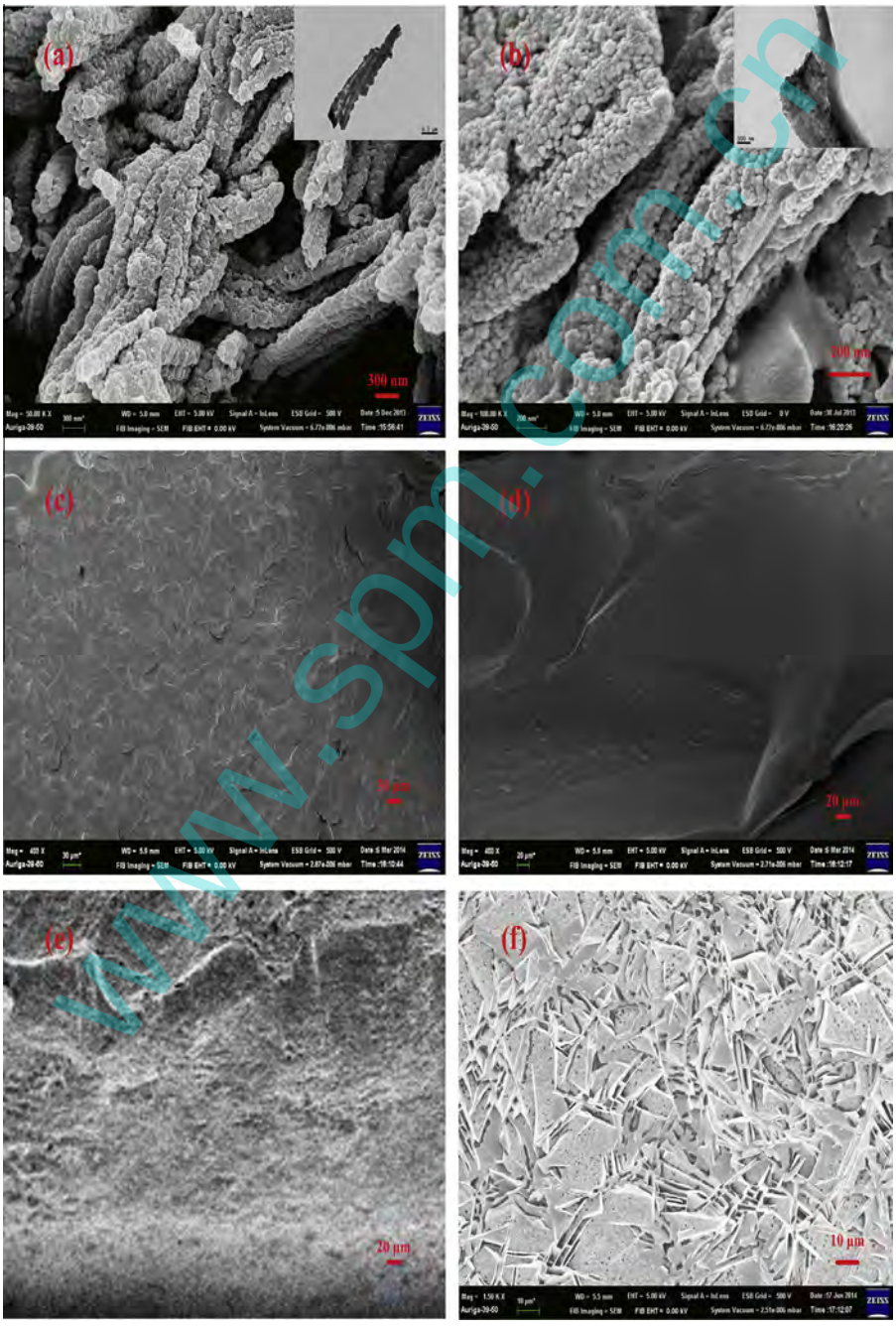

Fig. 3. SEM micrographs of (a) PANFDB, (b) PANFDBZnSt, (c) neat PP, (d) PPDB, (e) PPZnSt, and (f) PANFDBZnSt/PPZnSt.

miscible with PPZnSt. However, the obtained PANFDBZnSt/PPZnSt in the absence of additional DBSA became very fragile and owns poor mechanical strength due to lack of intermolecular connection. However, incorporation of additional DBSA in the melt-mixing can improve the connection between PANFDBZnSt and PPZnSt and mechanical properties effectively as already discussed in Fig. 1. Therefore, a polyblend system including PANFDBZnSt, DBSA, $Zn(St)_2$, and PP was set up and prepared by two stage kneading in Brabendar at various shear rates. Their SEM pictures were taken and discussed in the followings.

At low shear rate of 40 rpm in Fig. 4(a) for both 3000 and 50,000 magnifications, no significant aggregation of PANFDBZnSt in PPDBZnSt matrix can be seen in the SEM micrographs, indicating PANFDBZnSt are still randomly distributed with low shear force. It seems we need stronger shear force to reorganize the PANDBZSt in the dense PPDBZnSt matrix. Surprisingly, domino-like chips with thickness about 200 nm were seen in Fig. 4(b) when shear rate was increased to 60 rpm, which is much smaller than the flakes found in Fig. 3(e) for PANFDBZnSt/PPZnSt system. The prepared polyblend is much tougher and not fragile like PANFDBZnSt/PPZnSt which does not have additional DBSA. When shear rate as increased to 80–100 rpm in Fig. 4(c) and (d), the domino blocks are dominating in the matrix according to micrograph with 50,000 magnification shown in Fig. 4(c) and (d). At these shear rates, most of the plasticizers and some of the PPDBZnSt are mixed together and assembled with PANFDBZnSt into dominos. However, dissociation of the plasticizers and shrinkage, distortion of domino plates occurred when shear rate was higher than 100 rpm, increased to 120 and 140 rpm as seen in Fig. 4(e) and (f). The too strong shear spinning forces the separation of the low MW DBSA and $Zn(St)_2$ plasticizers from dominos which became thinner and distorted the domino plates as shown in 50,000 magnification of Fig. 4(e) and (f) and depicted in Scheme 3. In micrographs of 50,000 magnification of Fig. 4(e) and (f), we can clearly see more flat regions recovered from the gradual vanishing and thinning of dominos and more plasticizers slip back to PP matrix. The smoother morphology in Fig. 4(f) is very similar to Fig. 4(a) when the shear rate is low 40 rpm and no assembly occurred.

3.3.2. AFM

From AFM micrographs demonstrated in Fig. 5(a), we found that hairy rigid-rod PANFDBZnSt molecules build up pyramid-like structure with the lubrication of plasticizers in the PPDBZnSt matrix under shearing mixing at 40 rpm at 150 °C. Similarly, when shear rate was increased to 100 rpm at the same operating temperature in Fig. 5(b), these molecules were found to be able to erect and assemble into dominos depicted in Scheme 3. The erected dominos illustrate bright white color on the tops shown in Fig. 5. However, the dominos structure become thinner recovered to pyramid structure when shearing speed was increased to 140 rpm shown in Fig. 5(c), indicating the losing plasticizers at high speed shearing [12]

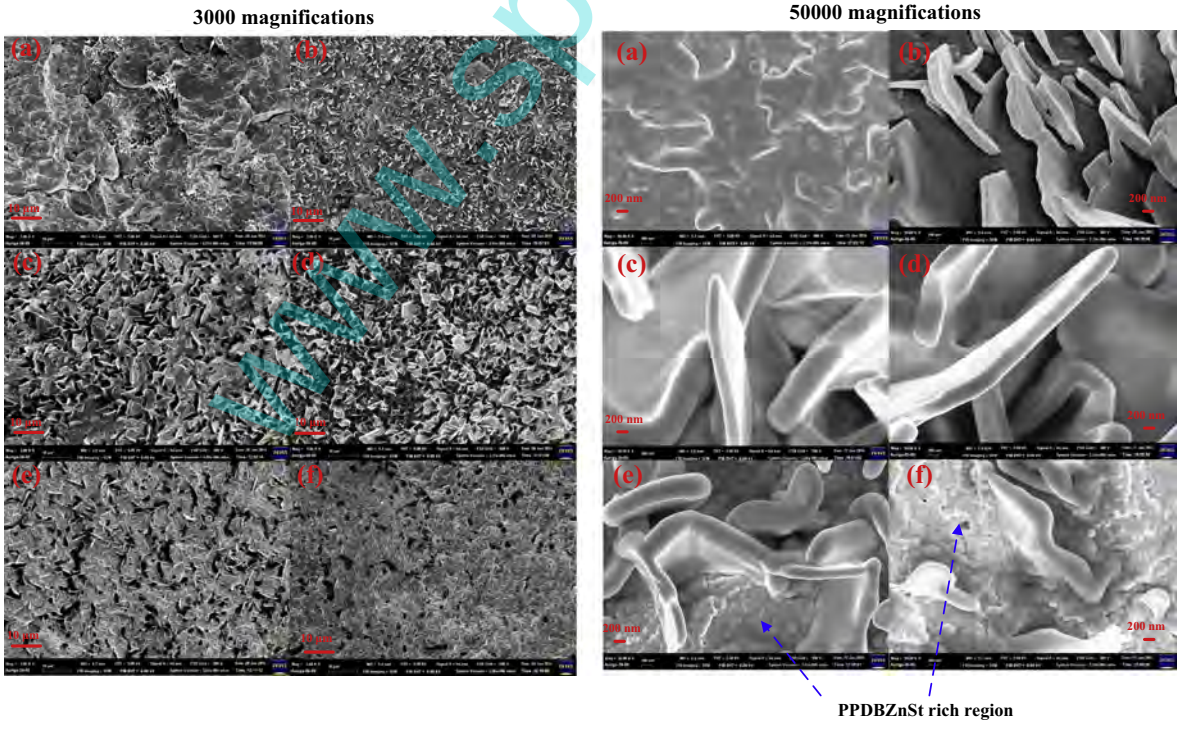

Fig. 4. SEM micrographs (3000 and 50,000 magnifications) of PANFDBZnSt/PPDBZnSt at (a) 40, (b) 60, (c) 80, (d) 100, (e) 120, and (f) 140 rpm.

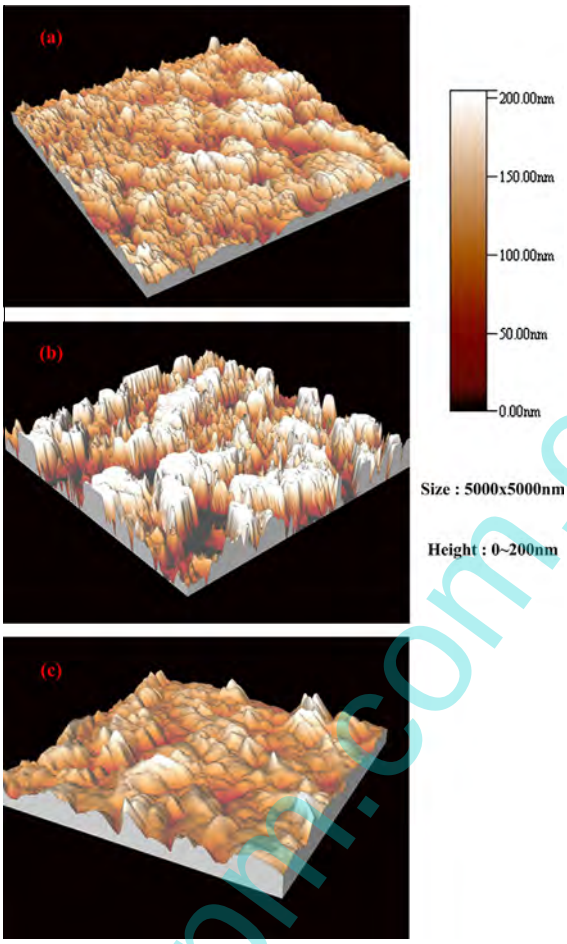

Fig. 5. AFM micrographs with depth difference expressed by color of PANFDBZnSt/PPDBZnSt at (a) 40, (b) 100, and (c) 140 rpm.

can destroy the domino structure. In other words, DBSA and $Zn(St)_2$ plasticizers and shear force play an important role for the formation of the erected dominos at some shearing speeds.

3.3.3. Infrared spectroscopy

The driving force of building a domino structure during shearing mixing of PANFDBZnSt with PPDBZnSt was characterized by comparing the IR-spectra of PANFDBZnSt before and after shear mixing with PPDBZnSt at shear rate of 60 rpm in Fig. 6 which clearly indicates the rocking of methylene group of PANFDBZnSt shifts from 797 to 802 cm^{-1} after melt-mixing. Since the attracting force is based on weak non-polar interaction, it is easily overcome by high speed of shearing, leading to the losing of DBSA, $Zn(St)_2$, and PANFDBZnSt from the dominos.

3.3.4. Differential scanning calorimetry

The thermograms of PANFDBZnSt/PPDBZnSt prepared at various shear rates were shown in Fig. 7 which demonstrates additional Tm at around 168 °C (Peak 2) except the Tm of neat PPDBZnSt at around 164 °C (Peak 1). Peak 2 was not found until shear rate reach 60 rpm and grew with shear rate but it decreased rapidly when shear rate was higher than 120 rpm according to Fig. 7. The obtained peaks in Fig. 7 were de-convoluted into Peak 1and 2, respectively and the individual heat of fusion was obtained by the integrated area of Peak 1 and 2, which were listed in the 1st and 2nd columns of Table 1. Since the sample weights were different, we calculate the ratio of Peak 1/Peak 2 listed in the 3rd column of Table 1 to illustrate the variation of relative percentage of different types of PP crystallines with shear rate. Similarly, the ratio decreased due to the growing of Peak 2 (domino building up) with shear rate at the beginning when shear rates were lower than 120 rpm and increased significantly at 140 rpm due to the losing ground of domino structure to the PP dominated matrix. In other words, the rising and sinking of the Peak 2 is related to the emerging and diminishing of the dominos, described in SEM micrographs. It seems the lamellar thickness of the PP crystalline inside of dominos is more compact than that of the neat PP, which results in the additional, higher Tm of Peak 2.

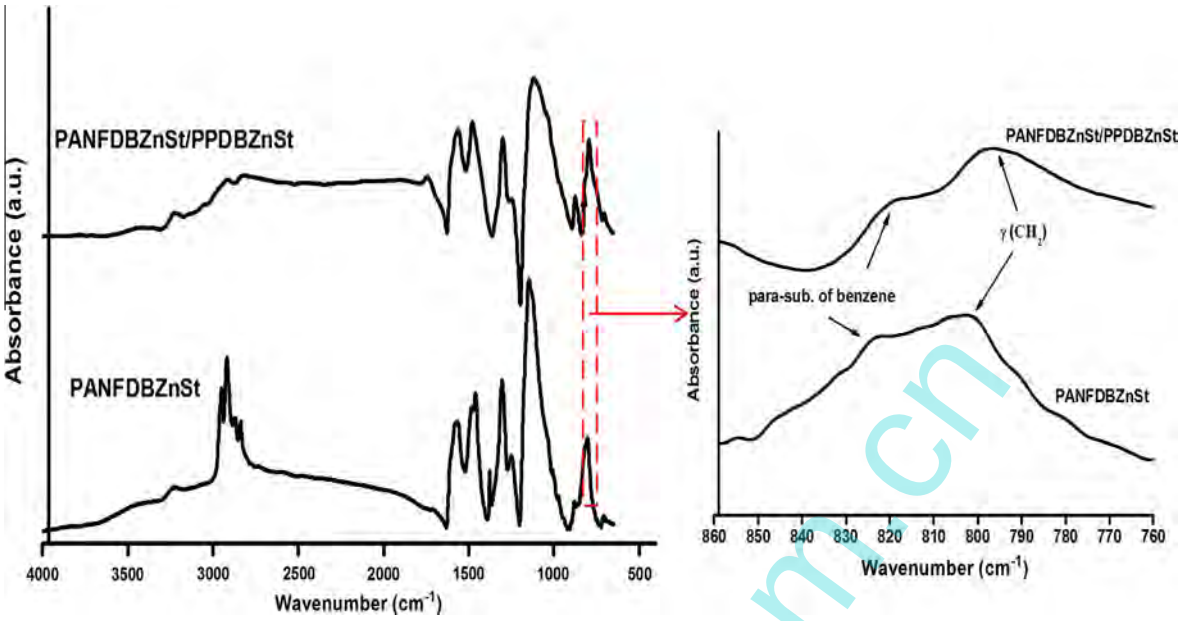

Fig. 6. IR-spectra of PANFDBZnSt and PANFDBZnSt/PPDBZnSt.

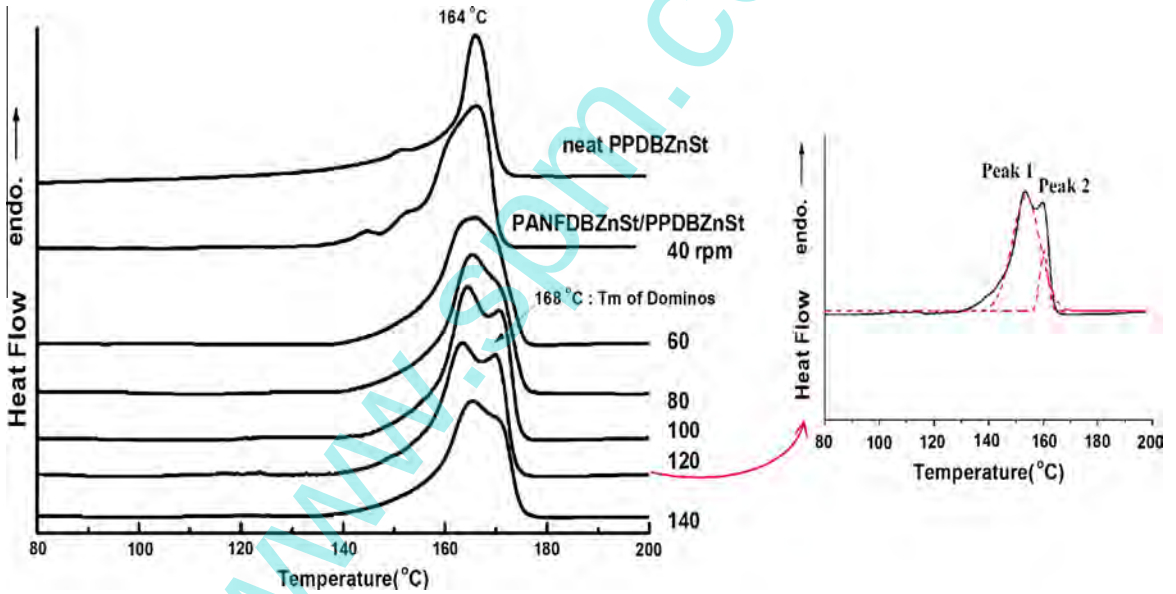

Fig. 7. DSC thermograms of PANFDBZnSt/PPDBZnSt prepared with various shear rates.

Table 1
Heat of fusion of PANFDBZnSt/PPDBZnSt at various shear rate.

Shear rate (rpm)	Peak 1 (J/g)	Peak 2 (J/g)	Peak 1/Peak 2
60	13.6	4.9	2.78
80	18.6	9.0	2.10
100	22.9	11.9	1.92
120	21.1	11.3	1.87
140	29.7	9.6	3.10

3.3.5. X-ray diffraction pattern

The x-ray diffraction patterns for neat PP or PANFDBZnSt/PPDBZnSt tell that PP whether it is melt-mixed with PANFDBZnSt or not is crystallized in α–monoclinic form whose characteristic planes including (110), (040), (130), (111), and (041) are illustrated in Fig.8. It can be found from the x-ray diffraction that (1 1 1) plane at $2\theta = 21^\circ$ seems to gradually dissociate at faster shearing. (110) plane was chosen to calculate the crystal size at different shear rates by the Debye-Scherrer equation. The obtained crystal sizes are listed in Table 2 which demonstrates huge crystals with sizes higher 10 nm are created after melt-mixing. Surprisingly, when PANFDBZnSt is melt-mixed with PPZnDBSt in the polyblend system, the crystal sizes were increased and became higher than 17 nm from 15.20 nm after blending according to 2nd column of Table 2. However, when shear rate is higher than 140 rpm at which the domino structure was gradually destroyed, the crystal size shrank to 13.99 nm which is even smaller, comparing to that of PPZnDBSt matrix as shown in Table 2. It seems the high shear rate also causes the dissociation of the crystals belonged to the PPZnDBSt matrix. The positions of (1 1 1) plane also shifted to higher angle with increasing shear rate as seen from the right inset figure of Fig. 8 and 3rd column of Table 2. It reveals that its d-spacing shrank and PP molecules came closer at high shear rates when part of the DBSA and $Zn(St)_2$ were spun off the crystalline structure.

Additional peak was found at the low-angled region around $2\theta = 7^\circ$ with a d-spacing equivalent to 12.84 Å when PANFDBZnSt was introduced and shear-mixed with PPDBZnSt according to Fig. 8. This large d-spacing and low angle peak originated from the assembly of PANFDBZnSt into the so-called layered structure depicted in Scheme 2 which can be easily formed with the accumulation of DBSA doped polyanilines [17,18] under the lubrication of DBSA and $Zn(St)_2$ plasticizers. This peak shifted to higher angle of $2\theta = 12^\circ$ (d-spacing = 7.37 Å) when shear rate reached 140 rpm, indicating the shortening of the layered distance (layer distance decreased from 12.84 to 7.37 Å) by losing some less bound PANFDBZnSt and DBSA and $Zn(St)_2$ plasticizers into PPDBZnSt matrix.

3.3.6. Resistivity variation with shear rate

The resistivity of PANFDBZnSt/PPDBZnSt prepared at various shear rates were measured and plotted with shear rate in Fig. 9 which demonstrates decreasing conductivity with shear rate, revealing that the rearrangement of conducting PANFDBZnSt under shearing did not cause any effective entanglements between PANFDBZnSt molecules but disconnected them. However, the PANFDBZnSt molecules did assemble and approached closer to each other into domino plates under the shearing as discussed in the above. It is believed the formation of highly concentrated PANFDBZnSt, conducting domino-plates did not percolate to increase conductivity but in the reverse way decreased it with increasing shear rates that break the conducting path of PANFDBZnSt. Only after the loss of plasticizers from the domino-plates at the highest shear rate of 140 rpm did the conductivity decrease moderately and some of the lower MW or loosely bound PANFDBZnSt molecules were spun out of the domino structure, mixing into the PPDBZnSt matrix. Briefly, although the conducting path can be disconnected with increasing shear rate, the intermolecular distance between PANFDBZnSt molecules became closer due to the loss of DBSA and $Zn(St)_2$ at higher shear rate, which compensate the disconnected effect. The plasticizer loss induces the thinning and distortion of the domino plates as well, as seen in Fig. 5.

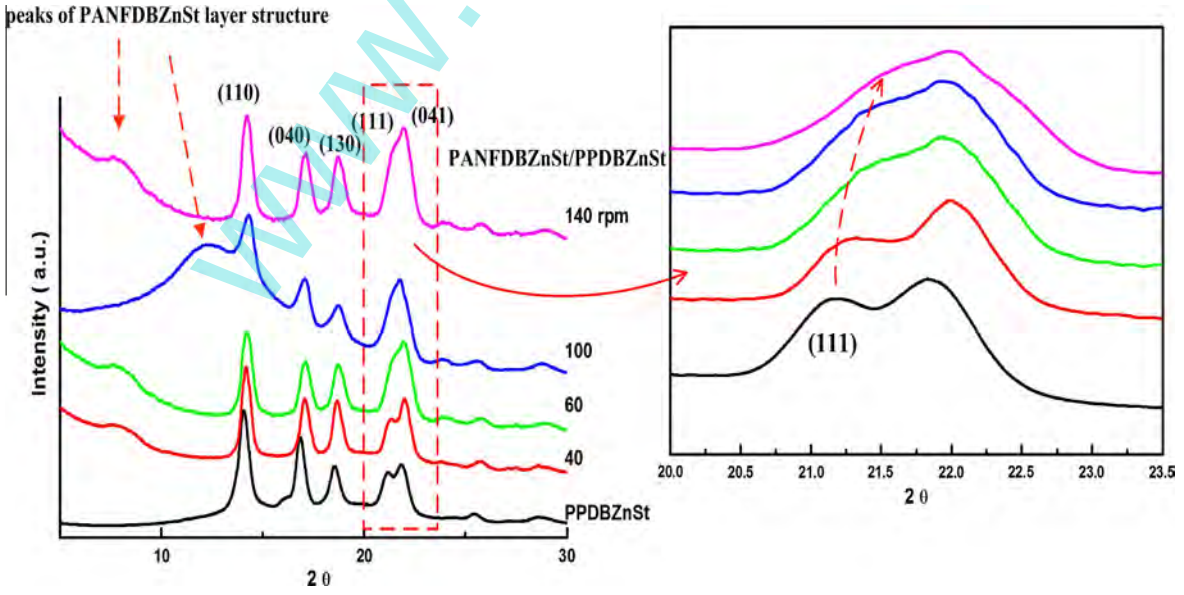

Fig. 8. X-ray diffraction patterns of PANFDBZnSt/PPDBZnSt at various shear rates.

Table 2
Crystal sizes and (1 1 1) positions of neat PPDBZnSt and polyblends.

Shear rate (rpm)	Size[a] (nm)	(1 1 1) plane (2θ)
Neat PPDBZnSt	15.20	21.18
PANFDBZnSt/PPDBZnSt		
40	17.14	21.32
60	17.20	21.42
100	17.16	21.44
140	13.99	21.51

[a] The average PP crystal size in the polyblends at each shear rate is calculated by the Debye-Scherrer equation based on the (1 1 0) reflection plane of PP crystalline. $d = \frac{k\lambda}{\beta \cos\theta}$ where k is a coefficient (0.9), λ is the wavelength of the X-rays (0.1541 nm for Cu Kα), β is the full-width half-maximum (FWHM) of the respective diffraction peak measured at $2\theta = 14°$ (converted to radians), and θ is the diffraction angle of the peak in degree.

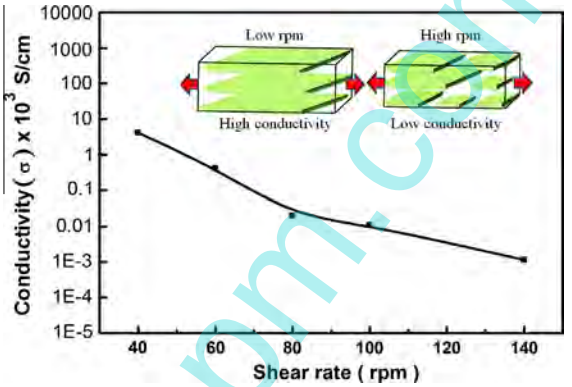

Fig. 9. Resistivity of PANFDBZnSt/PPDBZnSt at various shear rates.

4. Conclusions

Nanofibrous polyaniline (PANFDBZnSt) can be easily prepared in the presence of DBSA and $Zn(St)_2$ which behave as dopant and emulsifiers during polymerization. According to the morphological studies on the polyblends, PANFDBZnSt molecules are able to assemble into domino-like blocks at shear rate higher than 40 rpm when mixed with PP plasticized with DBSA and $Zn(St)_2$ (PPDBZnSt). The peculiar type of accumulation caused the increased intermolecular conjugation chain length of PANFDBZnSt in the polyblends and can be monitored by the growing λ_{max} in the Near-IR region at higher shear rates. Furthermore, the SEM and AFM pictures clearly show that the formation of domino blocks of PANFDBZnSt/PPDBZnSt at shear rates higher than 40 rpm. However, the domino blocks became thinner and part of them even disappeared gradually into the PPDBZnSt matrix due to the leaking of plasticizer at shear rate higher than 100 rpm. The domino blocks were found to be the combination of lots of parallel PANFDBZnSt layers, which contributed to the shifting of rocking methylene group in IR spectra and additional melting point in DSC thermograms and diffraction peak at low angle of X-ray diffraction. The conductivity decreased with shear rate due to the dis-entanglements of conducting PANFDBZnSt molecules with increasing shear rate.

The future work will focus on identification of the composition, and arrangement of the shear-induced dominos, evaluating the influence of the dominos on the other properties.

Acknowledgements

The authors would like to appreciate the financial support from Minister of Science and Technology in Taiwan, ROC through the Grants of: MOST 101-2622-E-151-017-CC3, MOST 103-2221-E-151-045, and MOST 104-2221-E-151-045. Another financial support from Tai-Flex Scientific company through the project: "Superparmagnetic composite based on iron nitride and other iron compounds" is also appreciated.

References

[1] K.S. Ho, K.H. Hsieh, S.K. Hung, T.H. Hsieh, Synth. Met. 107 (1999) 65–73.
[2] W.J. Lee, Y.J. Kim, S. Kanng, Synth. Met. 113 (2000) 237–243.
[3] R. Faez, M.A. De Paoli, Eur. Polym. J. 37 (2001) 1139–1143.
[4] M.E. Leyva, G.M.O. Bara, M.M. Gorelova, B.G. Soares, M. Sens, J. Appl. Polym. Sci. 80 (2001) 626–633.
[5] R. Faez, M.A. De Paoli, J. Appl. Polym. Sci. 82 (2001) 1768–1775.
[6] M.E. Leyva, G.M.O. Bara, B.G. Soares, Synth. Met. 123 (2001) 43–46.
[7] K.S. Ho, T.H. Hsieh, C.W. Kuo, S.W. Lee, J.J. Lin, Y.J. Huang, J. Polym. Sci. Chem. Ed. 43 (2005) 3116–3125.
[8] T.H. Hsieh, K.S. Ho, C.H. Huang, Y.Z. Wang, Z.L. Chen, Synth. Met. 156 (2006) 1355–1361.
[9] J. Ruokolainen, H. Eerika1inen, M. Torkkeli, R. Serimaa, M. Jussila, O. Ikkala, Macromolecules 33 (2001) 9272–9276.
[10] J. Hartikainen, M. Lahtinen, M. Torkkeli, R. Serimaa, J. Valkonen, K. Rissanen, O. Ikkala, Macromolecules 34 (2001) 7789–7795.
[11] L. Chao, Y.K. Han, B.Z. Hsieh, Y.J. Huang, T.H. Hsieh, C.M. Lin, S.Z. Lin, P.H. Tseng, K.S. Ho, J. Appl. Polym. Sci. 108 (2008) 3516–3522.
[12] L. Chao, Y.J. Huang, Y.K. Han, P.H. Tseng, T.H. Hsieh, C.M. Lin, K.S. Ho, Polym. Bull. 60 (2008) 847–853.
[13] S.Y. Shen, Y.J. Wu, K.S. Ho, T.H. Hsieh, T.H. Ho, Y.Z. Wang, et al, Polymer 52 (2011) 2609–2617.
[14] K.S. Ho, Synth. Met. 26 (2002) 151–158.
[15] K.S. Ho, T.H. Hsieh, C.W. Kuo, S.W. Lee, Y.J. Huang, C.N. Chuang, J. Appl. Polym. Sci. 103 (2006) 2120–2128.
[16] Y.Z. Wang, M.J. Tsai, T.H. Hsieh, P.H. Tseng, K.S. Ho, Polym. Int. (2005) (online published).
[17] Y.J. Wu, K.S. Ho, Y.W. Cheng, L. Chao, T.H. Hsieh, T.H. Ho, et al, Polym. Int. 62 (2013) 581–590.
[18] L. Chao, K.S. Ho, S.Y. Shen, H.Y. Pu, T.H. Hsieh, C.W. Kuo, et al, J. Appl. Polym. Sci. 127 (2013) 1853–1862.